Field deployable atomics package for an optical lattice clock

Kale, Yogeshwar; Singh, Alok; Gellesch, Markus; Jones, Jonathan; Morris, David; Aldous, Matthew; Bongs, Kai; Singh, Yeshpal

DOI:
10.1088/2058-9565/ac7b40

Document Version
Publisher's PDF, also known as Version of record

Citation for published version (Harvard):
Kale, Y, Singh, A, Gellesch, M, Jones, J, Morris, D, Aldous, M, Bongs, K & Singh, Y 2022, 'Field deployable atomics package for an optical lattice clock', *IOP Quantum Science and Technology*, vol. 7, no. 4, 045004. https://doi.org/10.1088/2058-9565/ac7b40

PAPER • **OPEN ACCESS**

Field deployable atomics package for an optical lattice clock

To cite this article: Yogeshwar B Kale *et al* 2022 *Quantum Sci. Technol.* **7** 045004

Quantum Science and Technology

PAPER

Field deployable atomics package for an optical lattice clock

Yogeshwar B Kale[1,*], Alok Singh[1], Markus Gellesch[1], Jonathan M Jones[1], David Morris[2], Matthew Aldous[2], Kai Bongs[1] and Yeshpal Singh[1,*]

[1] School of Physics and Astronomy, University of Birmingham, Birmingham, United Kingdom
[2] Cyber & Information Systems, Dstl Porton Down, Salisbury, United Kingdom
[*] Authors to whom any correspondence should be addressed.

E-mail: Y.Kale@bham.ac.uk and Y.Singh.1@bham.ac.uk

Keywords: optical lattice clock, strontium, ultra-cold atoms, field deployable, quantum technology

OPEN ACCESS

RECEIVED
8 April 2022

REVISED
10 June 2022

ACCEPTED FOR PUBLICATION
22 June 2022

PUBLISHED
5 July 2022

Abstract

An atomics package is the heart of any atom based quantum sensing device. Here we report on the realisation of a field deployable atomics package for alkaline earth atoms, e.g. Sr or Yb. In terms of size (∼121 L), weight (<75 kg) and power (∼320 W), it is the *smallest package to date* which is designed to load Sr atoms into an optical lattice. It consists of an ultra-high vacuum assembly (<4 L), lasers, magnetic field coils & optics required for cooling & trapping as well as a module for imaging & detection. The package can routinely produce ultra cold and dense samples of 1.6×10^5 ^{88}Sr atoms trapped in a 1D optical lattice in less than a second. Its robustness has been demonstrated by conducting two transportation campaigns within *out-of-the-lab* environments. This advancement will have impact not only on transportable optical clock development but also will influence the wider areas of quantum science and technologies, particularly requiring field deployable cold atom based quantum sensors.

1. Introduction

Over the last decade, optical atomic clocks have been one of the most crucial developments in the field of quantum science and technology [1–3]. Due to their unprecedented stability and uncertainty at 10^{-18} level, such clocks [4–6] can not only allow the redefinition of the SI unit of time [7–9], but can also play a key role in developing quantum technology for future information networks and communications [10]. They also permit geodetic applications such as measuring the gravitational potentials or chronometric levelling [11, 12] and monitoring changes in the geopotential caused by crust or upper mantle processes [13, 14]. Optical clocks are also important for fundamental science such as measuring the variations in the fundamental constants [15–18], the unification of the quantum theory and general relativity [19–22], searching for dark matter [23, 24] and detecting gravitational waves [25–27].

Optical clocks involve interrogation of an ultra-narrow transition in a neutral atom or ion using a highly stable narrow-linewidth laser as the local oscillator. For this task, the atomic/ionic samples need to be cooled down, tightly confined in the Lamb–Dicke regime, and shielded from the environmental influences. This is the function of the *atomics package* in any optical clock (in particular) or cold atom-based quantum sensor (in general). Figure 1 (left) shows basic building blocks of a typical optical clock. An *oscillator* (cavity locked narrow-linewidth clock laser) tuned to the desired clock frequency by interrogating the *reference* (ultracold trapped atomic/ionic ensembles) and by using appropriate feedback mechanism. The corrected optical frequency is *counted* by the frequency comb and down-converted to the corresponding RF signal for the various real world applications. It is crucial to have an accurate and stable *atomic/ionic frequency reference* for such a clock and hence the atomic package is at the heart of it.

Although any state-of-the-art optical clocks have exceptional performance in a well controlled lab-based environment, a host of applications lie outside the laboratory. Recently, a small number of transportable optical clock systems have been reported [28–32]. These systems are still very bulky and consume relatively large amounts of power for use in many field deployable applications. Development of true *field-deployable* optical clocks that are accurate and stable require overcoming the technological challenge of reducing their

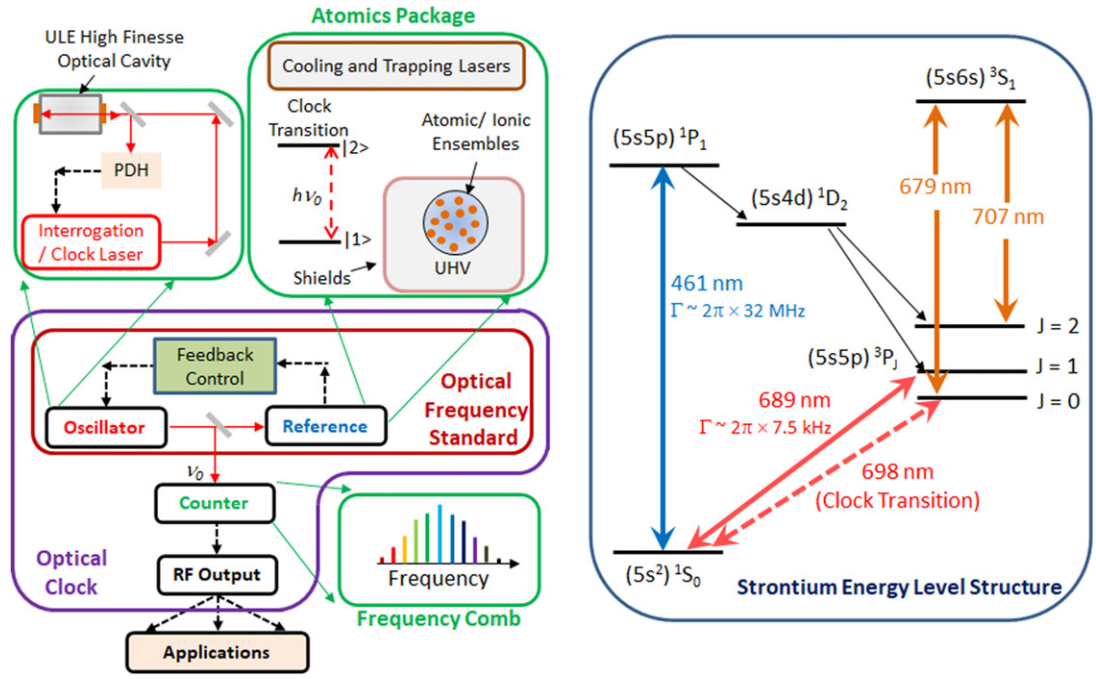

Figure 1. (Left) Basic building blocks of optical clocks. Abbreviations here are PDH—Pound–Drever–Hall locking, UHV—ultra high vacuum and ULE—ultra-low expansion; (right) relevant energy level diagram and corresponding transitions in strontium atoms.

size, weight and power (SWaP) as well as of realising a rugged architecture. Addressing these challenges will also expedite commercialisation of these technologies.

^{88}Sr is a good choice as an atomic reference for field-deployable clocks due to both its high natural abundance and recently proven compatibility with its fermionic counterpart [33]. A *stand-alone* atomics package which is capable of producing ultra-cold dense atomic samples trapped in optical lattices is vital in the realisation of field deployable quantum sensors, particularly those based on ultra cold atoms. In order to design and develop such package, the relevant strontium energy levels and the corresponding atomic transitions [34–36] should be kept in mind (see figure 1, left).

This paper discusses about the realisation and performance of a field deployable compact atomics package (CAP) for the application of a miniature, transportable optical lattice clock.

2. Structural features of the CAP

Considering transportability as the key criterion for field deployable quantum sensors, the CAP has been designed and developed such that it can be easily transported from one place to the other and quickly bought up to operational status. Its robust and rugged design is modular in nature, and includes the necessary sub-modules including compact ultra-high vacuum (UHV) assembly. The details are discussed in the following sections.

2.1. UHV assembly

The UHV assembly in the CAP uses a simplified and compact geometry without a dedicated Zeeman slower (see figure 2, left). The assembly is machined from titanium and divided into three major sections (i) strontium source, (ii) spectroscopy chamber and (iii) science chamber. The windows (or viewports) on the spectroscopy and science chambers are cold welded using high purity indium wire, providing a compact and permanent UHV seal. In order to avoid further bulkiness in the system, standard DN16CF flanges are preferred in building the system except at the two SAES NEXTorr Z100 pumps where DN35CF flanges are unavoidable. The pumps maintain $\sim 10^{-11}$ mbar as the static pressure in the science chamber, gauged by the ion pump current. A commercially available atomic dispenser (with operational power $\sim$ 10 W) is chosen as the source of the Sr atomic beam, rather than a bespoke effusive oven. In order to keep the atomic beam divergence as low as possible, we employ an extended circular aperture (diameter 4 mm) of length 5 mm. The horizontal pair of viewports immediately after the Sr source can be used for cross-beam spectroscopy and frequency stabilization of the cooling lasers. The science chamber is designed to form a magneto-optical trap (MOT) geometry with the help of a quad of prisms [37]. Here, a single, expanded and

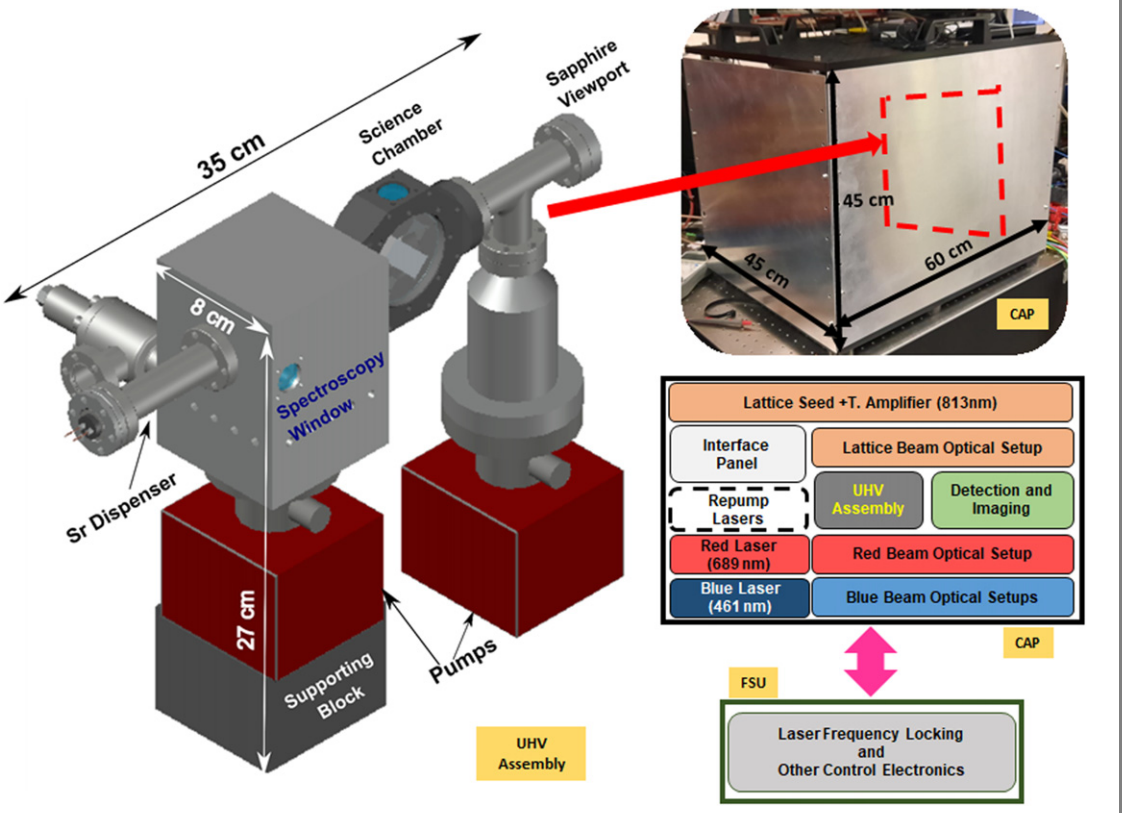

Figure 2. (Left) 3D rendering of the UHV assembly (right) the CAP for ultra-cold strontium atoms and simplified blocks of CAP, which make it multi-layered and modular suitable for transportability. The associated FSU enables frequency stabilisation of all the cooling and trapping lasers. It also provides control for all the optical, electrical and RF signals.

well-collimated beam is used to form a six-beam MOT geometry. A pair of viewports along the vertical axis of the science chamber allows the lattice beams to interact with cold atomic samples. The same windows can also be used to perform clock interrogation as well as other precision spectroscopic measurements. The viewport opposite to the atomic dispenser lets the Zeeman-like slowing laser beam in. This method takes advantage of the infringing magnetic field of the MOT coils. It is an effective method to increase the atom number without any significant increase in SWaP. Similar approach has been adapted in some of the previous works [38, 39]. The details of our method are discussed in section 3 and the corresponding results are presented in figure 6. In comparison to the previous works, we are using lower values of the operational power and detuning of Zeeman-like slowing beam. Over the time, strontium atoms can be deposited on this viewport drastically reducing the transmission of the slowing beam. By heating the sapphire window to approximately 200 °C, transmission of the Zeeman-like slowing beam can be restored. The UHV assembly has an arrangement to rigidly attach all the relevant optical mounts (e.g. MOT telescope, lattice beam assembly etc) providing robust optical alignment in the MOT region.

The end to end outer footprint of the UHV assembly is 35 cm × 8 cm × 27 cm with the net volume <4 L. To the best of our knowledge, this is the smallest UHV assembly used for any optical lattice clock setup to date.

2.2. Multi-layered modular structure

In order to make the CAP transportable, the necessary laser sources, optics, opto-mechanical and magnetic components needed to be integrated with the compact UHV assembly. This has been achieved by carefully designing a multi-layered structure of various optical setups related to the blue laser (461 nm), the red laser (689 nm), both the repump lasers (679 nm and 707 nm) and the lattice laser (seed + tapered amplifier, 813 nm). A pair of compact anti-Helmholtz coils, providing quadrupole magnetic field for magneto-optical trapping (total operational power dissipation <8 W), and three-axis field compensation coils (total operational power dissipation <3 W) are also attached to the science chamber. Due to their low power consumption, none of the coils require active cooling and can run continuously. The CAP contains charge-coupled device (CCD) camera (PCO Pixelfly-qe) for the imaging of cold atomic samples. It also includes a photomultiplier tube (PMT, Hamamatsu R12421-300) for the detection of atomic fluorescence during the experimental sequence. Telescopes for both the camera and the PMT use single lenses to form a $2f$ imaging system.

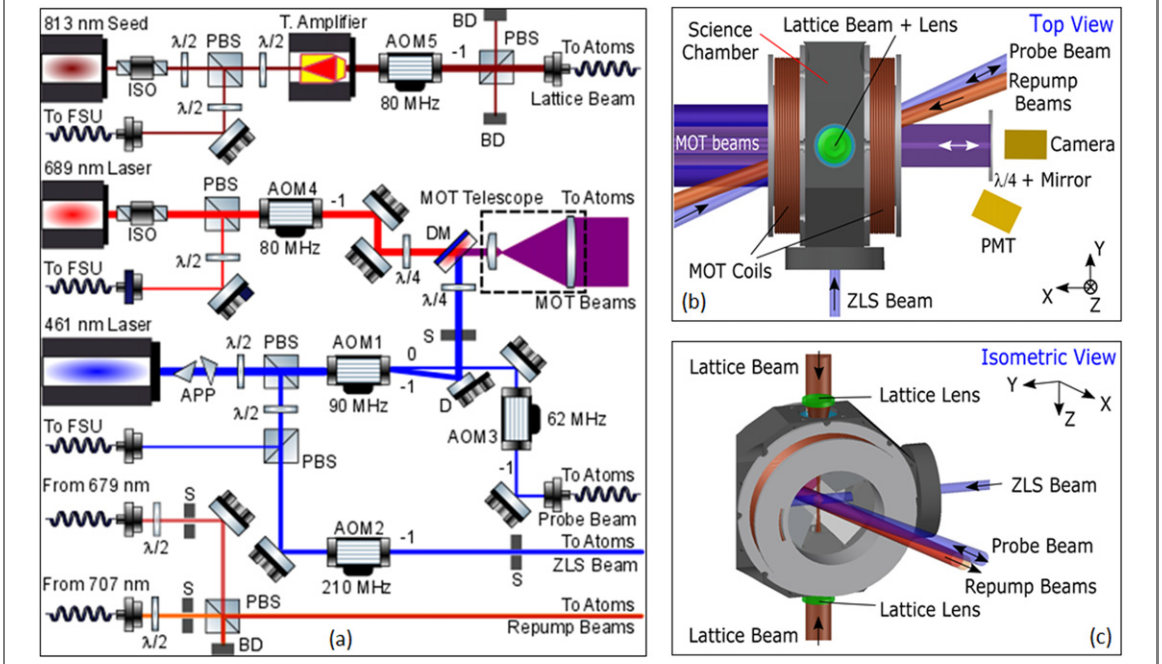

Figure 3. (a) Simplified schematics of the optical setup in CAP showing all the necessary components with labels as follows: AOMs—acousto-optic modulators, APP—anamorphic prism pair, BDs—beam dumps, D—D-shaped mirror, DM—dichroic mirror, ISO—optical isolator, $\lambda/2$—half waveplates, $\lambda/4$—quarter waveplates, PBSs—polarizing beam splitters, Ss—optical beam shutters, ZLS—Zeeman-like slowing. (b) Simplified 3D renderings of the science chamber (top view) in CAP demonstrating various beams interacting at the prism MOT region. The science chamber is surrounded by the MOT coils and (c) (isometric view) the vertical lattice beam is along Z-axis (gravity) and its size is exaggerated by ∼10 times only for the illustration purpose. The lattice beam is reflected back in order to form 1D lattice. For the detection and imaging, a retro-reflected probe beam is used as shown with a double headed arrow. For simplification, the MOT beams, camera and PMT are not shown in this view.

All the acousto-optic modulators (AOMs), optical beam shutters and coil magnetic fields are controlled via a single interface panel of the CAP. All the optical fibre interfaces also use the same interface panel.

The external frequency stabilization unit (FSU) is used to lock all the lasers and also to control all the optical, electrical and RF signals required for the experimental operation through the interface panel. This ensures minimal interference to the CAP during it is operation. The FSU includes home-built ultra-low expansion (ULE) optical cavity with finesse ∼20k to which the red laser (689 nm) is locked via the Pound–Drever–Hall technique. A lock bandwidth of >300 kHz achieves a laser linewidth estimated to be <700 Hz via the analysis of the in-loop error signal and direct beat note comparisons with other stable laser systems. The remaining lasers are locked to commercial wavelength meter (High Finesse WS U2).

2.3. Schematics of the optical setup in CAP

Figure 3(a) illustrates the simplified schematics of the optical setup in the CAP. A single commercial external cavity diode laser (ECDL, Toptica DL Pro, 461 nm, 110 mW) generates all the required blue laser beams such as MOT beam, a Zeeman-like slowing beam and a probe beam. A small part of the blue beam (<1 mW) is delivered through a fibre to the FSU for the frequency stabilization. The fraction of the blue beam is frequency shifted by AOM2 (−210 MHz) and used as the Zeeman-like slowing beam (power ∼ 3.5 mW at the sapphire window of the UHV assembly). The remainder of the blue beam passes through AOM1 (−90 MHz); the first order beam propagates toward the MOT telescope (∼40 mW power), whereas the 0th order beam is frequency shifted by AOM3 (−62 MHz) to provide a separate probe beam (fibre coupled in order to provide up to 1 mW power) for imaging & detection. This arrangement provides red detunings of ∼38 MHz for the first stage cooling at the $^1S_0$ to $^1P_1$ transition (see figure 1). It also provides red detuning of ∼10 MHz for the probe beams, with respect to the same cooling transition. The probe beam with operational power ∼297 μW and $1/e^2$ beam diameter ∼0.8 cm is retroreflected. The setup also includes optical delivery sub-modules for both the repump lasers i.e. 707 nm and 679 nm. The 679 nm repumper is a home-built compact interference filter laser (IFL) ECDL design [40] with output power of 20 mW, while the 707 nm is a commercial volume Bragg cavity laser (Sacher Micron: S1-0707-030-BFY) with output power of 30 mW. The lattice laser consists of a home-built IFL seed laser with output power 40 mW coupled into a commercially available tapered amplifier (TA, MogLabs MOA002) with output of 2 W. The TA output is filtered by an integrated amplified spontaneous emission filter. We have used two

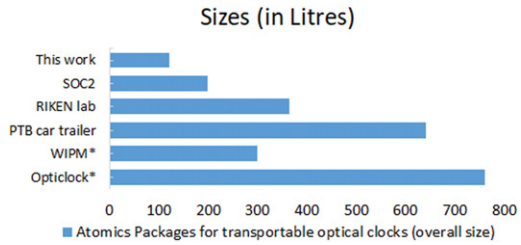

Figure 4. Comparison of the form factors for the reported atomics packages along with the CAP (this work) suitable for transportable optical clocks. WIPM and Opticlock are optical *ion* clocks (*) while others are optical *lattice* clocks.

Table 1. Estimated SWaP criteria for the atomics packages of the transportable optical clock systems.

Atomics package	Size (L)	Wt. (kg)	Power (W)	Reference
This work (Sr atoms)	121	75	320	
SOC2 (Sr atoms)	197	112	742	[28]
RIKEN lab (Sr atoms)	360	310	479	[31]
PTB car trailer (Sr atoms)	640	140	—	[30]
WIPM (Ca ions)	300	100	—	[29]
Opticlock (Yb ions)	760	100	—	[32]

types of lasers for the second stage cooling a home built ECDL in littrow configuration (28 mW) or Toptica TA pro (300 mW). The later one was used as *a lab based* alternative to the former. Both the lasers are interchangeable and are able to contribute in operation whenever required. All the lasers are locked by FSU to their respective transition frequencies. AOM4 which shifts the 689 nm beam down by 80 MHz is also used to artificially broaden the laser linewidth for the realisation of broadband red MOT. All the required, synchronized digital and analog and RF signals necessary to execute the experimental sequence are provided by the FSU. Figures 3(b) and (c) shows simplified 3D renderings (top and isometric views) of the beam geometries around the MOT region. The figure shows that the Zeeman-like slowing beam enters from the sapphire view port, which counter propagates the atomic beam. Both the blue and red MOT beams combined at the dichroic mirror are expanded to 40 mm diameter (FWHM) using a single MOT telescope such that they are slightly larger than the prism MOT region inside the science chamber. Suitable 3D printed masks (not shown) are used in the MOT telescope to reduce light scattering inside the science chamber. Both the repump beams ($1/e^2$ diameter $\sim$ 10 mm) co-propagate from the back to the front of the science chamber. In order to form a vertical 1D-optical lattice, the 813 nm beam enters (downward) into the science chamber from the top view port. After passing through a lens ($f = 40$ mm) the lattice beam is tightly focused at the MOT position. While retroreflecting (upwards) on the same path, the lattice beam is again focused at the same spot by another identical lens. At the focus, the waist is $\sim$32 μm. As both lattice lenses are mounted on micrometer translation mounts (Thorlabs SM1ZA, not shown), the individual foci can be precisely adjusted during the lattice optimization phase.

2.4. SWaP budget for the CAP

Figure 4 is a comparative representation of the atomics packages of the transportable optical clocks reported by various groups around the world. This includes transportable systems with both cold neutral atoms and cold ions. The WIPM [29] and Opticlock [32] are developed for *optical ion* clock systems whereas rest of the packages mentioned here, [28, 30, 31] including the CAP, are developed for *optical lattice* clock systems. In the previously reported works, the *atomics packages are* mainly defined as the UHV assembly and do not include the laser sources, light distribution modules, detection hardware and imaging modules etc. In the process of miniaturization of quantum sensors, the definition of atomics package requires further inclusion of the above mentioned modules. As per our knowledge, the CAP is the smallest package till date for *an optical lattice* clock setup. The corresponding SWaP budgets of the reported atomics packages along with the CAP are tabulated in table 1.

3. Operation, results and discussion

A typical experimental timing sequence for the setup is illustrated in figure 5. There are five different phases which are discussed here one by one.

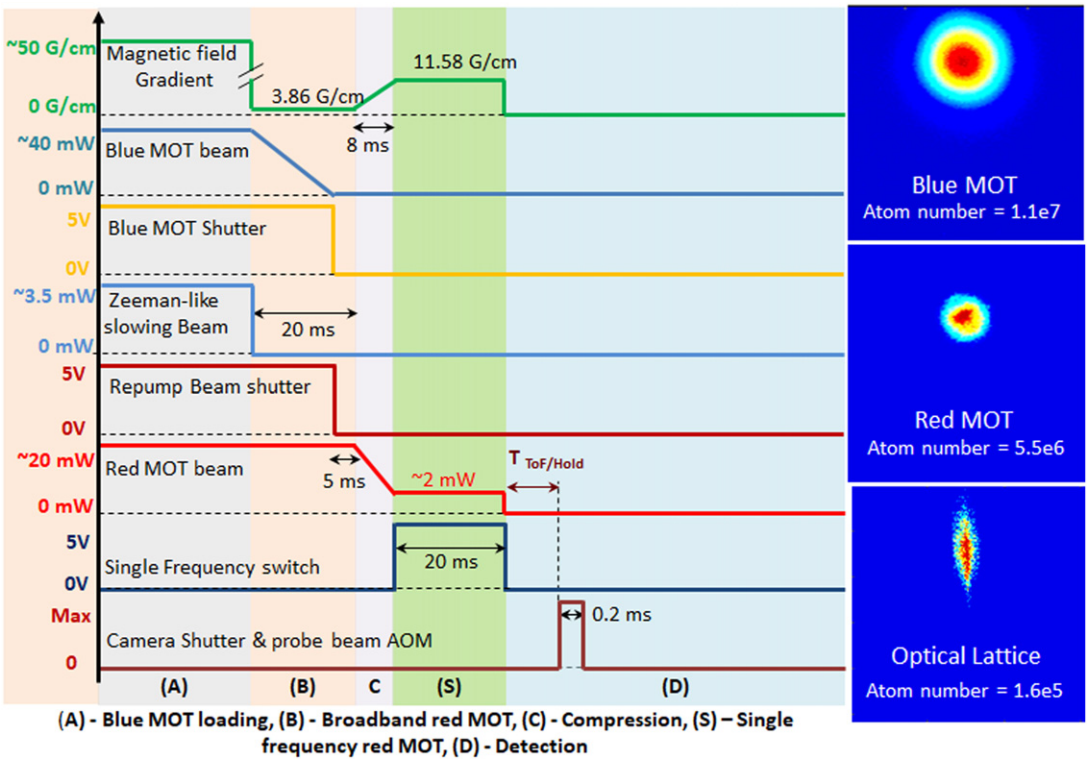

Figure 5. The experimental timing sequence in CAP. (Inset: images recorded *in situ* for blue MOT, single frequency red MOT and for the atoms in lattice at $T_{\mathrm{Hold}} = 45$ ms.) The lattice is always kept on, hence not shown here for the sake of clarity.

(A) *Blue MOT loading:* here, ^{88}Sr atoms are loaded from the atomic beam pre-slowed down with a Zeeman-like slowing beam. Both the repump beams are active in order to bring the lost atoms back to the cooling cycle (see figure 1, right). The atom numbers in the blue MOT are optimized with respect to the Zeeman-like slowing beam's detuning and power (see figure 6, left). It has been observed that the CAP can load up to 1.7×10^7 atoms into the first stage cooling with ∼10 mW power of the Zeeman like slowing beam. We are able to observe up to 5.2 times increase in the blue MOT atom number due to the Zeeman-like slowing beam. In our case, the enhancement in atom number due to the Zeeman-like slowing beam is limited by the available power. Thus, for this paper, we have used power of 3.5 mW and red detuning of 158 MHz for the Zeeman-like slowing beam. At the end of this phase, approximately 1.1×10^7 atoms are loaded in the blue MOT (with temperature ∼ 3 mK). The inset of the figure 6, left, shows a typical loading curve of the blue MOT with loading time ∼580 ms as recorded by the PMT. At this stage,we also have estimated the magnetic trap lifetime τ in the metastable $^3P_2$ state is ∼592 ms (see figure 6, right). This is done using the trap loading curve ($\tau \sim 232$ ms) shown in the inset. The faster loading of atoms in the magnetic trap may be due to the interaction of MOT atoms with the atomic beam or their interaction with Sr atoms in other states like $^1D_2$ or $^3P_{1,2}$ [41, 42].

(B) *Broadband red MOT:* in this phase, atoms are transferred from the blue MOT to a broadband red MOT acting on the $^1S_0$–$^3P_1$ transition. Here the blue MOT beam power is ramped down from 40 mW to 0 mW in 15 ms, both the repump beams are blocked using a shutter and the field gradient is lowered to 3.86 G cm^{-1}. The MOT coil's switching off time is ∼400 μs. Ramping down the blue MOT beams intensities allows the atoms to cool down further by reducing re-absorption of spontaneously emitted photons during the first stage as well as allows a smooth transfer into the second stage cooling cycle. In our case, quick switching the MOT beams off results in ∼32% of atom transfer into red MOT, while ramping the beams down in 15 ms results into 50% atom transfer. The broadband red MOT is run for 5 ms. At this stage, the 689 nm laser linewidth here is artificially broadened to ∼1 MHz, with modulation frequency 20 kHz for an optimal atom transfer to broadband red MOT (temperature ∼ 20 μK).

(C) *Compression:* further, the broadband red MOT is compressed by ramping up the field gradient from 3.86 G cm^{-1} to 11.58 G cm^{-1} in 8 ms and simultaneously lowering the red MOT beam power from 20 mW to 2 mW (intensity ∼ 550 μW cm^{-1}). The spatial compression of the red MOT helps to achieve higher atom densities, and lowering the beam intensity cools down the atom temperature in single frequency MOT phase. [43].

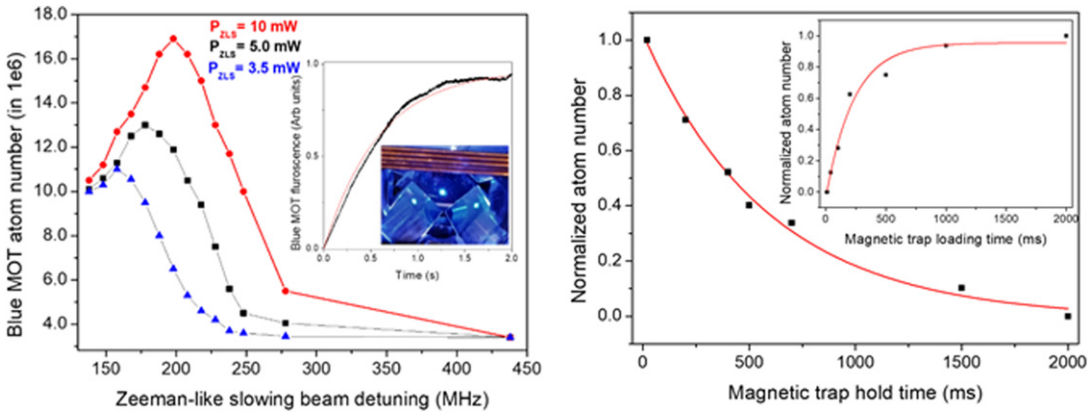

Figure 6. (Left) Blue MOT atom numbers as a function of Zeeman-like slowing beam detuning for various values of beam power and (inset) a typical blue MOT loading curve and blue MOT image in CAP (for the Zeeman-like slowing beam power 3.5 mW and detuning of 160 MHz from the $^1S_0$–$^1P_1$ transition of ^{88}Sr), (right) magnetic trap (in $^3P_2$ state) lifetime and magnetic trap loading (inset) in CAP ($1-\sigma$ error bars are too small to be visible).

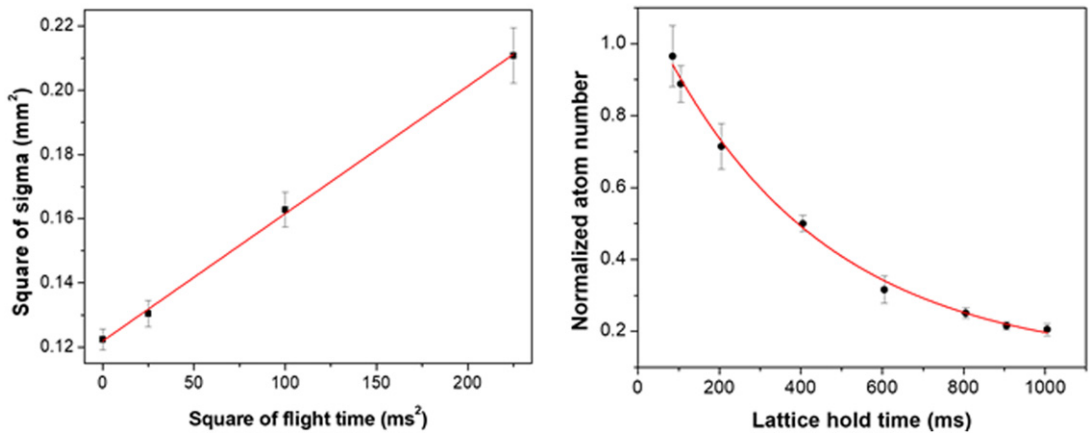

Figure 7. (Left) ToF of the single frequency red MOT atoms for the temperature measurement ($T \sim 5\ \mu$K), (right) decay of lattice trapped atoms as function of the lattice hold time estimating lifetime of ∼406 ms at operational dispenser current of 7.75 A.

(S) *Single frequency red MOT:* here, artificial broadening of the red laser linewidth is withdrawn to transfer atoms into a single frequency red MOT, enabling narrow-line laser cooling for 20 ms. As mentioned in (B), the transfer efficiency of cold atoms from the first stage cooling to the narrow-line cooling is ∼50%. The time-of-flight (ToF) measurements has been used to estimate the temperature of the cloud (figure 7, left) [44]. The expanding MOT cloud size σ Gaussian radius width and flight time (t) are connected to temperature (T) by $\sigma^2(t) = {\sigma_0}^2 + (k_B T t^2/m)$, where, σ_0 is cloud size at zero ToF, k_B is Boltzmann constant, m is the atomic mass of ^{88}Sr. The square of the size of single frequency red MOT is plotted as a function of the square of the flight time. Typically we trap about 5.5×10^6 atoms at $\sim 5\ \mu$K in a single frequency red MOT.

(D) *Detection:* during the ToF measurements, all the magnetic and optical fields are turned off. The sequence is repeated by varying the flight time. The probe beam and the CCD camera are simultaneously turned on (for 200 μs) for the detection and imaging of the atoms.

In order to load the atoms into the 1D lattice, the lattice beam is turned on and the laser is locked to the magic wavelength (813.427 57(62) nm) [45] using the FSU. The entire sequence is repeated by varying the lattice hold time. Nearly 1.6×10^5 atoms from the single frequency red MOT stage are successfully loaded into the 1D lattice potential (after the hold time of 45 ms) with the depth of ∼110 μK. Lowering the lattice depth further to approximately 22 μK, the CAP is still able to trap $\sim 2.9 \times 10^4$ atoms. This can help to reduce AC stark shifts during the optical lattice clock operation. At an operational atom dispenser current of 7.75 A, we have achieved the lattice lifetime of 406 ms (see figure 7, right). The current life time is limited by the background atoms in the science chamber. Typical images recorded by the CCD camera for the blue

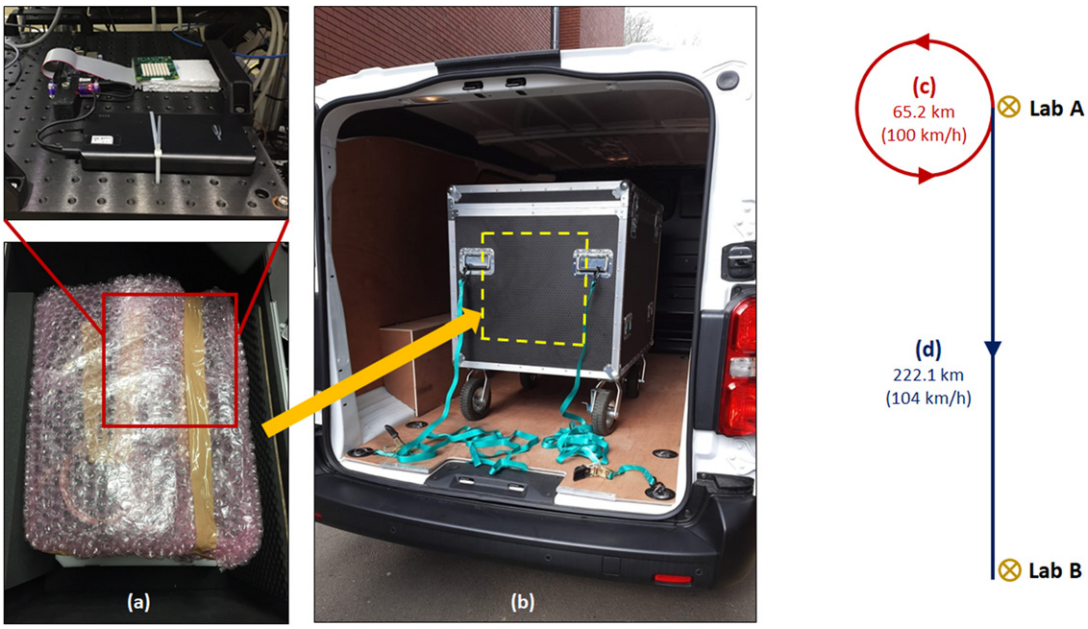

Figure 8. Pre-transportation phase: (a) CAP protected by anti-static wrapping is placed inside the fight case (inset: prior to this, the data logger with its power bank is mounted on top of the CAP), (b) flight case with the CAP inside is at back of van for short-distance transport scenario. Transportation phase: (c) representative route of the shorter city traffic round trip campaign, distance covered around 65.2 km with maximum speed of 100 km h^{-1} and (d) representative route of the medium distance intercity campaign, distance covered around 222 km with maximum speed of 104 km h^{-1}.

MOT (*in situ*), the single frequency red MOT (*in situ*) and for the lattice trapped atoms (at 45 ms of the lattice hold time) are shown in figure 5.

4. Transportation and restarting of CAP

Transportability is crucial for the development of next-generation, field deployable optical lattice clocks [46]. The required level of robustness may vary on the type of transport required and can span scenarios from ground transport in a standard commercial vehicle, to a launch into space as a dedicated payload. Here, we consider ground transport as this constitutes a common initial step for use of CAP outside the lab environments. Hence, further to the optimization procedure, the CAP is subjected to two *out-of-the-lab* transport scenarios (see figure 8). In detail: (i) a short-distance inner-city round trip campaign in the proximity to the Lab A site and (ii) a medium distance intercity campaign (from Lab A to Lab B). Lab B is situated at around 221 km from Lab A. The campaigns were planned in three main phases and with well-defined procedure protocols are followed for its successful transportation:

(1) *Pre-transportation phase:* for both campaigns, the CAP box is disconnected from the FSU by removing all connectors from the interface panel. A small home-buit data logger consisting of the required sensors is mounted firmly on top of the CAP box. The sensors (inertial measurement unit of a Rasberry Pi Sense Hat) record parameters of interest, i.e. acceleration, rotation, and ambient magnetic fields in the direction of x, y, and z axis as well as angular orientation. Additional sensors on the Sense HAT measure relative humidity and atmospheric pressure during the transportation campaigns. The CAP is carefully covered with anti-static wrap material and is placed in a flightcase where it is cushioned with suitable foam materials. For the short-distance transportability trial in proximity to the lab, the flightcase was then loaded into a commercial van (Vauxhall Vivaro Panel 'Dynamic', 120 PS, diesel, six-speed manual transmission) and fastened with suitable ratchet straps at the four corners of the loading bay.

(2) *Transportation phase:* for the first measurement campaign i.e. the short-distance scenario in city traffic, the speed of the vehicle varied from 30–50 km h^{-1}. Peak travel speeds for this trial were around 100 km h^{-1}, however, only for shorter durations of less than 10 min. Overall, this transportability test run covered a distance of 65.2 km. The route for the inner-city trial is chosen so that the CAP is exposed to various conditions including degraded road surfaces, construction sites, road bumps, and stop-and-go traffic during its transportation.

For the medium-distance transport campaign to the facilities at Lab B, the CAP is transported via motorways which allows a significantly longer exposure to the speeds of 100–104 km h^{-1}. The focus on this

Table 2. Maximum parametric deviations measured[a] during the transportation campaigns.

Sr. No.	Change in parameter (maximum)	Round trip campaign	Intercity campaign
1	Acceleration (x)	1.23 g	0.94 g
2	Acceleration (y)	0.96 g	0.63 g
3	Acceleration (z)	1.53 g	0.24 g
4	Magnetic field (x)	0.58 G	1.10 G
5	Magnetic field (y)	0.95 G	0.65 G
6	Magnetic field (z)	2.21 G	1.33 G

[a]The values are within the accuracy limit and calibration error of the mounted sensors.

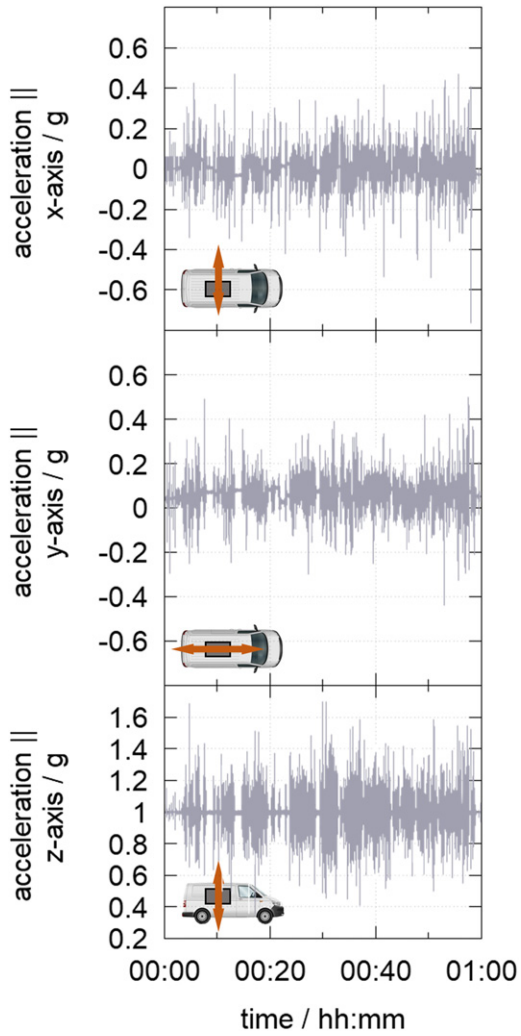

Figure 9. Time traces of the acceleration (in x, y and z axis) experienced by the CAP during the roundtrip campaign.

intercity transportability trial is to emulate conditions of a delivery of the CAP from one site to another. Data recorded during the two measurements campaigns is summarised in table 2.

One can infer that the CAP experiences up to about 2.21 G of stray magnetic fields. The CAP also experiences a maximum acceleration of 1.53 g during its round trip transportation campaign. It also records a relative humidity change of more than 55% during the intercity transportation campaign. Figure 9 represents the data recorded by the CAP mounted sensor for the accelerations experienced in x, y and z axis during the roundtrip transportation campaign. Similar data has been recorded for the intercity campaign (not shown here).

The CAP is exposed to changes in temperatures during the campaigns, which is approximately 8 °C above the lab temperature at 21 °C and temperature gradients of 0.25 °C per minute. The design ensures that the optical breadboards and enclosures in the package serve as passive heat sinks.

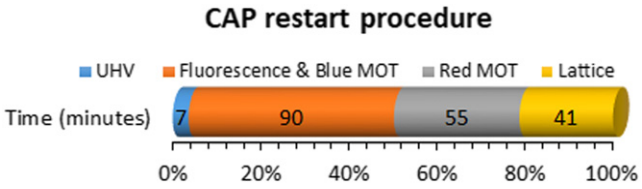

Figure 10. Post-transportation phase: breakdown of the typical time required to complete the restart procedure for the CAP.

(3) *Post-transportation phase:* in this phase, the CAP is unloaded from the vehicle at its desired destination. This phase also successfully demonstrates the *rapid restart procedure* which brings the CAP back to its optimized operational state in just over 3 h.

All the crucial stages are achieved as per the schedule in the protocol and a desired number of atoms is re-loaded into 1D lattice. Four main stages are involved in the restart procedure:

Stage (I)—the pressure check in the UHV assembly is conducted and Sr dispenser is activated.

Stage (II)—all the required interfaces are established between the CAP and the FSU through its interface panel. The laser sources are checked for acceptable powers are stabilised to their required frequencies. The cross-beam spectroscopy is performed to see an atomic fluorescence in the science chamber. The magnetic fields are turned on and consequently blue MOT is realized within 90 min.

Stage (III)—compensation fields are optimized and the atoms in blue MOT are transferred to red MOT. The temperature of atoms are confirmed by ToF measurements.

Stage (IV)—the lattice beams are opened and the atoms from the red MOT are trapped into the 1D lattice potentials. The time dedicated for each stage is graphically presented in figure 10.

It need to make sure that the locking collars of all the kinematic mounts are fasten before a field trials. The first (round trip) transportation campaign also helped us to upgrade our *rapid restart procedure* protocol for the intercity campaign.

5. Conclusion and future perspective

We were able to design, develop and demonstrate the operation of a robust transportable atomics package which is proficient in producing the ensemble of ^{88}Sr ultra-cold atoms. To the best of our knowledge, this represents the smallest footprint for an optical lattice clock set up to date. With the repetition of $<$1 s, the system is able to generate about 1.6×10^5 ultra-cold atoms confined to 1D optical lattices. The lattice lifetime has been measured to be 406 ms which can further be increased by lowering the dispenser current. We have also performed transportation and restart sequences in order to demonstrate its suitability for field deployable applications. By inserting optical elements such as EOM and AOM in the available space, the CAP can easily be modified for the fermionic ^{87}Sr isotope. This can be achieved while retaining the overall functionality and operation intact. The main expected change will be the reduction in atom number approximately by ten fold but still maintaining sufficient atom number for the suitability of all the applications including optical lattice clocks.

Such a *stand-alone* package based on ultracold strontium atoms could form the basis for an optical lattice clock as well as for the large momentum transfer atom interferometers [47] in *out-of-the-lab* environments. This will be crucial step towards the realization of a *high bandwidth quantum navigation system* [48]. The package could also find potential applications in the broader areas of quantum technologies such the development of portable quantum simulators [49] or quantum computing platforms [50, 51]. *Optical lattice based* portable quantum processors platforms can able to perform high fidelity computational operations similar to recently developed commercial superconducting processor like *Sycamore* [52]. Such a quantum simulator can prove its suitability in fields like the study of quantum many body systems in condensed matter [53], long-range interactions [54], synthetic gauge fields [55], and special unitary group of n degrees i.e. SU(N) systems [56] for the fermionic alkaline-earth species.

Acknowledgments

Authors acknowledge the funding from the UK Defence Science and Technology Laboratory (DSTLX-1000095040) and the Quantum Hub for Sensors and Metrology (EPSRC funding within Grant EP/M013294/1). The contents include material subject to Dstl ©Crown copyright 2022.

Data availability statement

All data that support the findings of this study are included within the article (and any supplementary files).

ORCID iDs

Yogeshwar B Kale https://orcid.org/0000-0001-5824-7426

References

[1] Diddams S A *et al* 2001 *Science* **293** 825
[2] Katori H 2002 *Proc. 6th Symp. on Frequency Standards and Metrology* vol 323 ed P Gill
[3] Wilpers G, Binnewies T, Degenhardt C, Sterr U, Helmcke J and Riehle F 2002 *Phys. Rev. Lett.* **89** 230801
[4] Nicholson T L *et al* 2015 *Nat. Commun.* **6** 6896
[5] Ushijima I, Takamoto M, Das M, Ohkubo T and Katori H 2015 *Nat. Photon.* **9** 185
[6] Brewer S M, Chen J-S, Hankin A M, Clements E R, Chou C W, Wineland D J, Hume D B and Leibrandt D R2019 *Phys. Rev. Lett.* **123** 033201
[7] Gill P 2011 *Phil. Trans. R. Soc.* A **369** 4109
[8] Margolis H 2014 *Nat. Phys.* **10** 82
[9] Riehle F, Gill P, Arias F and Robertsson L 2018 *Metrologia* **55** 188
[10] Riehle F 2017 *Nat. Photon.* **11** 25
[11] McGrew W F *et al* 2018 *Nature* **564** 87
[12] Delva P, Denker H and Lion G 2019 *Relativistic Geodesy* (*Fundamental Theories of Physics* vol 196) (Berlin: Springer) p 25
[13] Bondarescu R, Schärer A, Lundgren A, Hetényi G, Houlié N, Jetzer P and Bondarescu M 2015 *Geophys. J. Int.* **202** 1770
[14] Tanaka Y and Katori H 2021 *J. Geod.* **95** 93
[15] Stadnik Y V and Flambaum V V 2015 *Phys. Rev. Lett.* **114** 161301
[16] Sanner C, Huntemann N, Lange R, Tamm C, Peik E, Safronova M S and Porsev S G 2019 *Nature* **567** 204
[17] Huntemann N, Lipphardt B, Tamm C, Gerginov V, Weyers S and Peik E 2014 *Phys. Rev. Lett.* **113** 210802
[18] Godun R M *et al* 2014 *Phys. Rev. Lett.* **113** 210801
[19] Walsh D, Carswell R F and Weymann R J 1979 *Nature* **279** 381
[20] Will C M 2014 *Living Rev. Relativ.* **17** 4
[21] Brax P 2017 *Rep. Prog. Phys.* **81** 016902
[22] Bongs K and Singh Y 2020 *Nat. Photon.* **14** 408
[23] Derevianko A and Pospelov M 2014 *Nat. Phys.* **10** 933
[24] Wcisło P *et al* 2018 *Sci. Adv.* **4** eaau4869
[25] Kolkowitz S, Pikovski I, Langellier N, Lukin M D, Walsworth R L and Ye J 2016 *Phys. Rev.* D **94** 124043
[26] Su J, Wang Q, Wang Q and Jetzer P 2018 *Class. Quantum Grav.* **35** 085010
[27] He F and Zhang B 2020 *Eur. Phys. J.* D **74** 94
[28] Bongs K *et al* 2015 *C. R. Phys.* **16** 553
[29] Cao J, Zhang P, Shang J, Cui K, Yuan J, Chao S, Wang S, Shu H and Huang X 2017 *Appl. Phys.* B **123** 112
[30] Grotti J *et al* 2018 *Nat. Phys.* **14** 437
[31] Takamoto M, Ushijima I, Ohmae N, Yahagi T, Kokado K, Shinkai H and Katori H 2020 *Nat. Photon.* **14** 411
[32] Opticlock 2021 *Meas.: Sensors* **18** 100264
[33] Origlia S *et al* 2018 *Phys. Rev.* A **98** 053443
[34] Loftus T H, Ido T, Boyd M M, Ludlow A D and Ye J 2004 *Phys. Rev.* A **70** 063413
[35] Kock O, He W, Świerad D, Smith L, Hughes J, Bongs K and Singh Y 2016 *Sci. Rep.* **6** 37321
[36] Bowden W *et al* 2019 *Sci. Rep.* **9** 11704
[37] He W 2017 Towards miniaturized strontium optical lattice clock *PhD Thesis* University of Birmingham
[38] Poli N, Schioppo M, Vogt S, Falke S, Sterr U, Lisdat C and Tino G M 2014 *Appl. Phys.* B **117** 1107
[39] Golovizin A, Tregubov D, Mishin D, Provorchenko D and Kolachevsky N 2021 *Opt. Exp.* **29** 36744
[40] Baillard X, Gauguet A, Bize S, Lemonde P, Laurent P, Clairon A and Rosenbusch P 2006 *Opt. Commun.* **266** 609
[41] Stuhler J, Schmidt P O, Hensler S, Werner J, Mlynekn J and Pfau T 2001 *Phys. Rev.* A **64** 031405
[42] Nagel S B, Simien C E, Laha S, Gupta P, Ashoka V S and Killian T C 2003 *Phys. Rev.* A **67** 011401
[43] Katori H, Ido T, Isoya Y and Kuwata-Gonokami M 1999 *Phys. Rev. Lett.* **82** 1116
[44] Brzozowski T M, Maczynska M, Zawada M, Zachorowski J and Gawlik W 2002 *J. Opt. B: Quantum Semiclass. Opt.* **4** 62
[45] Akatsuka T, Takamoto M and Katori H 2010 *Phys. Rev.* A **81** 023402
[46] Gellesch M, Jones J, Barron R, Singh A, Sun Q, Bongs K and Singh Y 2020 *Adv. Opt. Technol.* **9** 313
[47] Rudolph J 2020 *Phys. Rev. Lett.* **124** 083604
[48] Feng D 2019 *IOP Conf. Ser.: Earth Environ. Sci.* **237** 032027
[49] Georgescu I M, Ashhab S and Nori F 2014 *Rev. Mod. Phys.* **86** 153
[50] Heinz A *et al* 2020 *Phys. Rev. Lett.* **124** 203201
[51] Madjarov I S *et al* 2020 *Nat. Phys.* **16** 857
[52] Arute F *et al* 2019 *Nature* **574** 505
[53] Hofstetter W and Qin T 2018 *J. Phys. B: At. Mol. Opt. Phys.* **51** 082001
[54] Olmos B, Yu D, Singh Y, Schreck F, Bongs K and Lesanovsky I 2013 *Phys. Rev. Lett.* **110** 143602
[55] Wall M L, Koller A P, Li S, Zhang X, Cooper N R, Ye J and Rey A M 2016 *Phys. Rev. Lett.* **116** 035301
[56] Zhang R, Cheng Y, Zhang P and Zhai H 2020 *Nat. Rev. Phys.* **2** 213